



**ISTITUTO NAZIONALE DI FISICA NUCLEARE**

**Laboratori Nazionali del Sud**

---

**INFN/TC-06/07**  
**14 March 2006**

**SIMULATIONS AND MEASUREMENTS ABOUT THE  
ELECTROMAGNETIC PROPERTIES FOR THE CYLYNDRICAL  
CAVITY OF THE SERSE ION SOURCE**

F. Maimone<sup>1</sup>, D. Mascali<sup>2</sup>, F. Consoli<sup>2</sup>, S. Barbarino<sup>3</sup>, L. Celona<sup>2</sup>, G. Ciavola<sup>2</sup>,  
S. Gammino<sup>2</sup>

<sup>1</sup> Università di Catania – Dipartimento di Ingegneria Informatica e delle Telecomunicazioni  
Via A. Doria, 6 – 95125 Catania – ITALY

<sup>2</sup> Istituto Nazionale di Fisica Nucleare – Laboratori Nazionali del Sud  
Via S. Sofia, 62 – 95123 Catania - ITALY

<sup>3</sup> Università di Catania – Dipartimento di Fisica e Astronomia  
Via S. Sofia, 64 – 95123 Catania – ITALY

**Abstract**

The electron heating process in an ECR ion source is affected by the electromagnetic properties of the plasma chamber and by the coupling properties of microwave generators with the chamber itself.

Hence, the theoretical and experimental study of these properties is very important in order to improve the transfer of the electromagnetic waves energy to the plasma electrons.

In this report an analytical and numerical characterization of the SERSE plasma chamber resonant modes is presented along with an experimental and numerical characterization of the microwave coupling.

PACS.: 41.20.Jb, 52.35.Hr, 50.50.Sw, 52.70.Ds, 52.70.Gw

## 1. Introduction

At the INFN-LNS, the ECR ion source SERSE is employed to produce relatively low currents of high charge states ions to be accelerated by the K-800 superconducting cyclotron for nuclear physics experiments. The electromagnetic characterization of the plasma chamber together with the waveguide branching up to the DC-break represent a fundamental step to have a better understanding of the coupling between the microwave generators and the plasma chamber. The code used for such modelization is the CST MICROWAVE STUDIO™ (CST MWS) which is able to calculate the resonant frequencies of the vacuum chamber and determine the scattering parameters to analyze the coupling between the cavity and the microwaves ports.

Figure 1 shows a scheme of the SERSE ion source with a detailed view of the injection and extraction flanges. In the injection flange there are the gas inputs, the hole for the biased disk (used to increase the amount of electrons in the plasma), and the microwaves ports (WR62 type) named WG1 and WG2. This flange it is also drilled with holes for pumping; the diameter of the holes is below 8/4 in order to minimize microwave leaks and plasma formation outside the chamber. Similar holes are also present in the extraction side, with aperture for the ion beam extraction.

Then it is possible to model the chamber with a resonant cylindrical cavity with apertures in both end flanges. The first part of the report will present the results of the numerical calculations with the CST MICROWAVE STUDIO™ code [1], whereas the second one present the experimental results and a comparison between simulated and observed data.

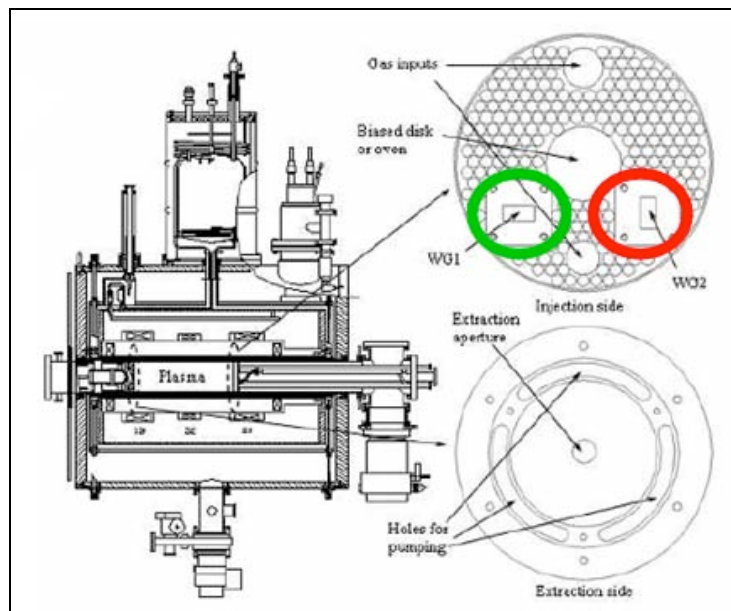


Figure 1: Scheme of the SERSE ion source and injection and extraction flanges.

## 2. Numerical simulations

From the theory of the resonant cavities we know that inside a cylindrical cavity the propagation of electromagnetic waves is allowed only for a discrete set of frequencies given from the equation:

$$\omega = c \sqrt{\left(\frac{r\pi}{l}\right)^2 + h^2} \quad (1)$$

where  $c$  is the speed of light,  $r$  is an integer and  $h$  is the eigenvalue of the Helmholtz equation:

$$\nabla^2 \phi + h^2 \phi = 0 \quad (2)$$

where  $\phi$  is the longitudinal component of the magnetic field for TE modes, or the longitudinal component of the electric field for the TM modes.

If we consider a cylindrical cavity with circular section with radius  $a$  and length  $l$ , the equations that determine the allowed frequencies for TM and TE modes are respectively [2]:

$$f_{nvr} = \frac{c}{2\pi} \sqrt{\left(\frac{x_{nv}}{a}\right)^2 + \left(\frac{r\pi}{l}\right)^2} \quad (3)$$

$$f_{nvr} = \frac{c}{2\pi} \sqrt{\left(\frac{x'_{nv}}{a}\right)^2 + \left(\frac{r\pi}{l}\right)^2} \quad (4)$$

where:  $x_{nv}$  and  $x'_{nv}$  are respectively the zeros of order  $v$  of the Bessel functions of order  $n$  and its first derivative. In a metallic resonant cavity there are losses due to the dissipation of electromagnetic energy on its walls. These losses determine an attenuation of the electromagnetic field when the external excitation is removed. For this reason we introduce the *quality factor*  $Q_0$ , defined as the ratio between the total energy, averaged on a period, contained in the cavity, and the mean energy dissipated in a period.

According with the previous formalism, we define two different expression to calculate  $Q_0$ , for TM and TE modes respectively:

$$\begin{aligned}
 Q_0 &= \mu \sqrt{\frac{\pi \sigma f_{nv} r}{\mu_p}} \frac{1}{\left[ \frac{2}{l} + \frac{1}{a} \right]} & r \neq 0 \\
 Q_0 &= \mu \sqrt{\frac{\pi \sigma f_{nv} r}{\mu_p}} \frac{1}{\left[ \frac{1}{l} + \frac{1}{a} \right]} & r = 0
 \end{aligned}
 \tag{5}$$

$$Q_0 = a \mu \sqrt{\frac{\pi \sigma f_{nv} r}{\mu_p}} \frac{\left\{ \left[ \left( \frac{r\pi}{l} \right)^2 + h_{nv}^2 \right] \left[ 1 - \left( \frac{n}{h_{nv} a} \right)^2 \right] \right\}}{\left[ h_{nv}^2 + 2 \frac{r^2 \pi^2 a}{l^3} + \frac{r^2 \pi^2 n^2}{h_{nv}^2 a l^2} \left( \frac{1}{a} - \frac{2}{l} \right) \right]}
 \tag{6}$$

In these equations  $\mu_p$  is the magnetic permittivity of the cavity metallic walls (with conductivity  $\sigma$ ).

A first model to simulate the cylindrical cavity with the same dimensions of the SERSE chamber is a cylinder which length is 450 mm and the radius is 65 mm without holes and filled with air ( $\epsilon_r = 1$ ).

If we suppose to haven't any energy losses, the CST MWS eigenmode solver simulator is very efficient to calculate the resonant frequencies. This solver calculates the first N frequencies and the related field diagrams [1]. In this way we can perform a comparison between the theoretical values obtained by solving equations (3) and (4),[3] and the values obtained by the numerical simulations with the CST MWS code.

The following report presents the results obtained by considering only the SERSE vacuum chamber as a cylindrical cavity without taking into account the perturbations introduced by the holes in the injection and extraction flanges.

Taking into account that the SERSE plasma chamber is aluminum made ( $\sigma = 3.77 \cdot 10^7$  [S/m]), table 1 summarizes the comparison between the first 20 resonant frequencies and their relative  $Q_0$  factors obtained by the CST MWS simulation and the theoretical values.

Hereinafter the relative difference between simulated and theoretical values is presented, obtained by subtracting the simulated value to the theoretical one and dividing by the latter.

Table 1: Comparison between simulation and theoretical values for the first 20 modes.

|    | Mode       | Frequency [HZ]<br>Simulation | Frequency [Hz]<br>Theoretical value | $Q_0$<br>Simulation | $Q_0$<br>Theoretical value |
|----|------------|------------------------------|-------------------------------------|---------------------|----------------------------|
| 1  | $TE_{111}$ | 1.39175002e+009              | 1.39197046e+009                     | 2.1477e+004         | 2.147463675e+004           |
| 2  | $TE_{112}$ | 1.50657203e+009              | 1.50680259e+009                     | 2.4058e+004         | 2.405928249e+004           |
| 3  | $TE_{113}$ | 1.68056512e+009              | 1.68084538e+009                     | 2.7847e+004         | 2.785686543e+004           |
| 4  | $TM_{010}$ | 1.76500198e+009              | 1.76526966e+009                     | 2.8990e+004         | 2.911217902e+004           |
| 5  | $TM_{011}$ | 1.79615027e+009              | 1.79642267e+009                     | 2.5926e+004         | 2.607670317e+004           |
| 6  | $TM_{012}$ | 1.88650291e+009              | 1.88679800e+009                     | 2.6507e+004         | 2.672459447e+004           |
| 7  | $TE_{114}$ | 1.89747674e+009              | 1.89787860e+009                     | 3.2297e+004         | 3.234869821e+004           |
| 8  | $TM_{013}$ | 2.02813798e+009              | 2.02849546e+009                     | 2.7431e+004         | 2.770993075e+004           |
| 9  | $TE_{115}$ | 2.14426675e+009              | 2.14489162e+009                     | 3.7079e+004         | 3.710953678e+004           |
| 10 | $TM_{014}$ | 2.21118464e+009              | 2.21167263e+009                     | 2.8592e+004         | 2.893402434e+004           |
| 11 | $TE_{211}$ | 2.26607027e+009              | 2.26658251e+009                     | 2.1572e+004         | 2.175528805e+004           |
| 12 | $TE_{212}$ | 2.33834214e+009              | 2.33886053e+009                     | 2.2461e+004         | 2.265208433e+004           |
| 13 | $TE_{116}$ | 2.41171738e+009              | 2.41269389e+009                     | 4.1827e+004         | 4.186224604e+004           |
| 14 | $TM_{015}$ | 2.42623949e+009              | 2.42695544e+009                     | 2.9914e+004         | 3.030953835e+004           |
| 15 | $TE_{213}$ | 2.45404723e+009              | 2.45459889e+009                     | 2.3851e+004         | 2.406086788e+004           |
| 16 | $TE_{214}$ | 2.60737741e+009              | 2.60801797e+009                     | 2.5588e+004         | 2.587491667e+004           |
| 17 | $TM_{016}$ | 2.66550963e+009              | 2.66657916e+009                     | 3.1323e+004         | 3.177061786e+004           |
| 18 | $TE_{117}$ | 2.69361254e+009              | 2.69509524e+009                     | 4.6428e+004         | 4.645696139e+004           |
| 19 | $TE_{215}$ | 2.79209856e+009              | 2.79291507e+009                     | 2.7711e+004         | 2.797911184e+004           |
| 20 | $TM_{110}$ | 2.81174989e+009              | 2.81267565e+009                     | 3.6700e+004         | 3.674760264e+004           |

Figures 2 and 3 show very good agreement between results of the simulations and theoretical values. In particular it can be noticed that for the resonating frequency the difference is less than 0.055%, whereas for the quality factor the difference is less than 1.5%.

However the figures show that increasing frequency the difference between the two values grows up; in particular we notice that for each mode the values obtained from the simulations are higher than the analytical ones. This probably means that could be a sort of systematic error that further studies on the mathematical aspects of the CST MWS eigenmode solver could eliminate.

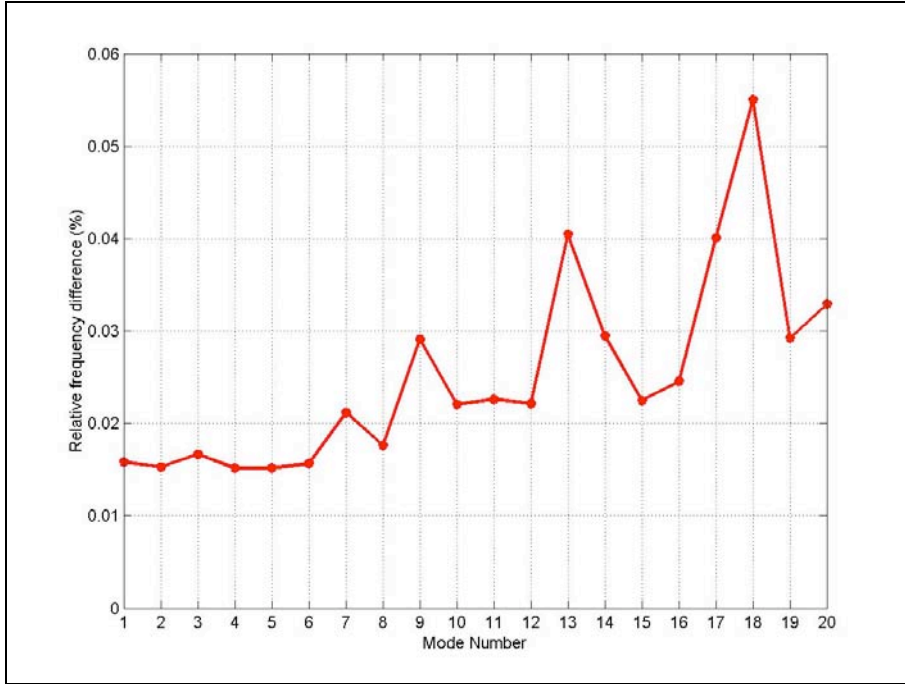


Figure 2: Relative difference between theoretical and simulated frequency resonance (first 20 modes).

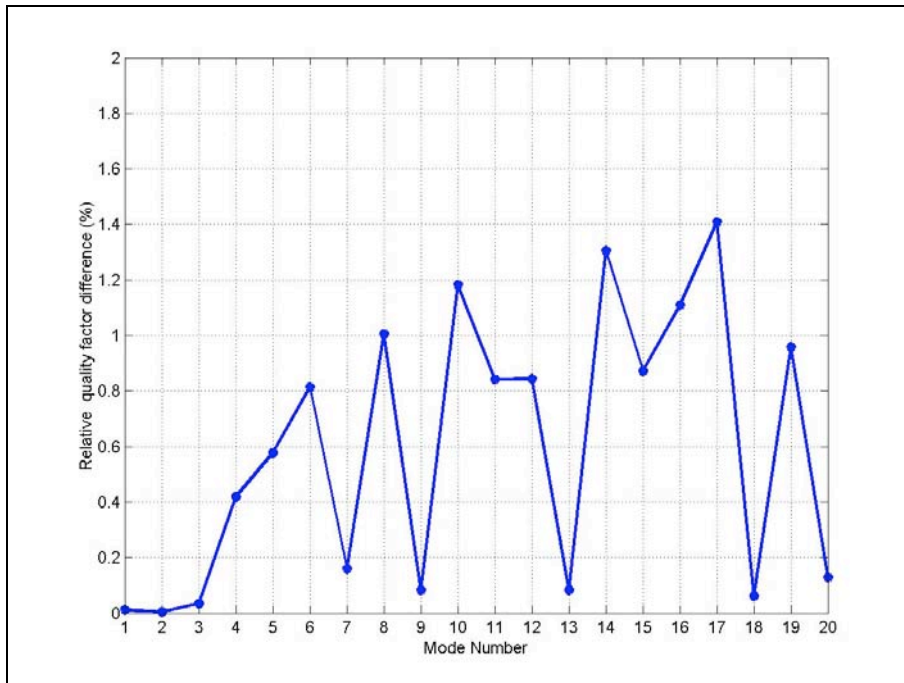


Figure 3: Relative difference between theoretical and simulated quality factor (first 20 modes).

Our goal is to achieve a reasonable agreement between theoretical values and simulations up to the SERSE working frequencies (18 GHz). In this case we will be able to compare our calculation with the S-parameters measurements on the source as described in the following paragraph. CST MWS simulations also allow the determination and plotting the field distribution inside the vacuum chamber for each resonant mode.

Figure 4 shows the electric field diagram for the mode  $TE_{111}$ , i.e. the first resonant mode.

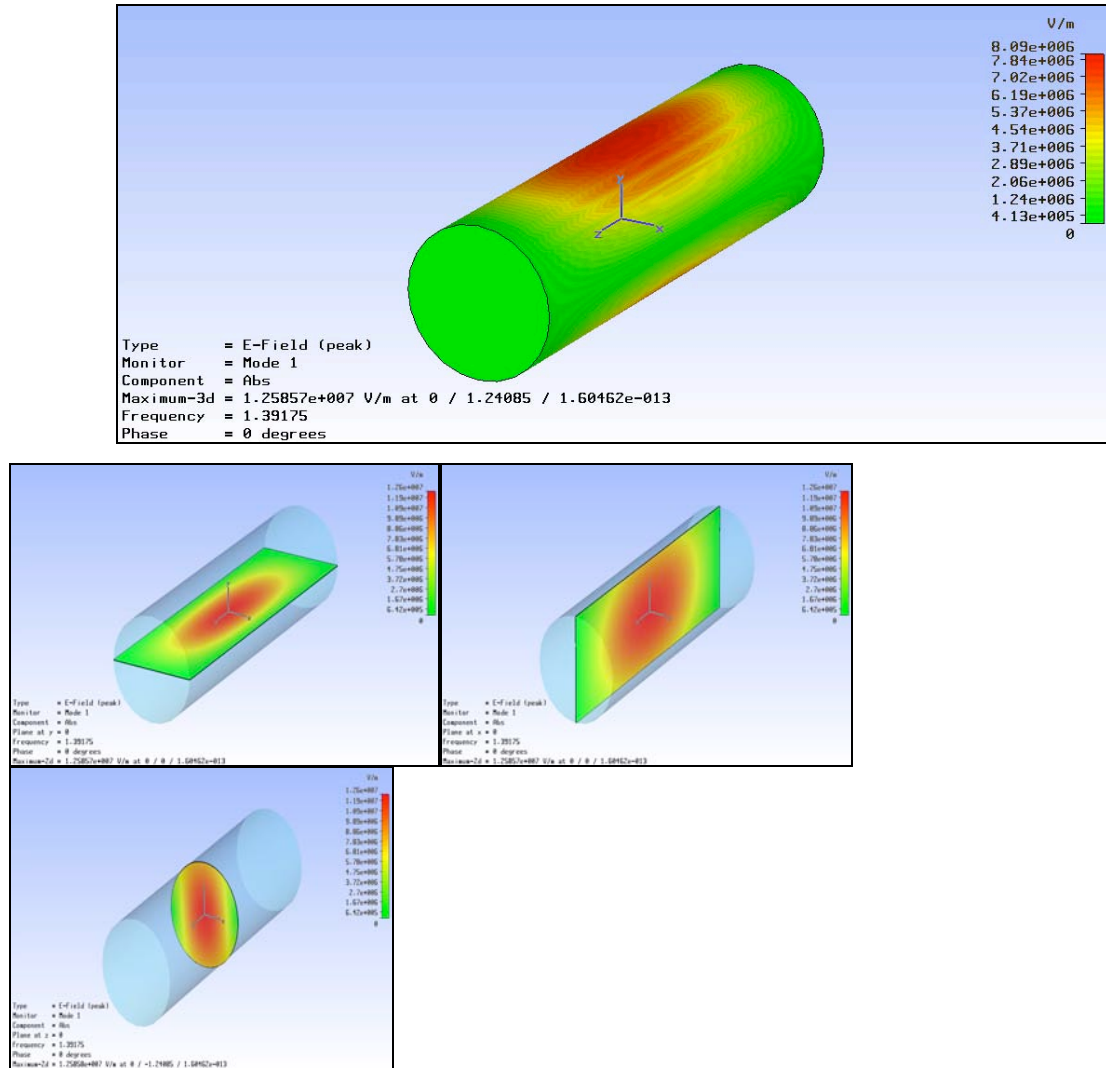


Figure 4: Mode  $TE_{111}$ : trend of the absolute value of the electric field on the external part of the structure and on the three planes: x-z, y-z e x-y.

Starting from these results, it is interesting to formulate a new model of the plasma chamber, considering the holes for microwaves injection, ion extraction, vacuum system and gas injection.

However the specific characteristics of CST MWS eigenmode solver, which do not permit to perform simulations with open structures, will certainly complicate such a job. For this

reason further studies will be necessary in order to define a model able to represent the real plasma chamber structure even using other codes (e. g. Ansoft HFSS™).

### 3 Experimental results

In order to characterize the SERSE plasma chamber in terms of mode distribution and then to study the coupling of different microwave generators, some measurements have been performed by using a vector network analyzer (Agilent N 5230 A PNA L-Series) able to work up to 50 GHz. These measurements have been performed in absence of plasma inside the source plasma chamber.

The waveguides WG1 and WG2 (see figure 1) were connected respectively with the port 1 and 2 of the network as shown in figure 5. The results reported in the following pages represent the scattering parameters measured by the instrument.

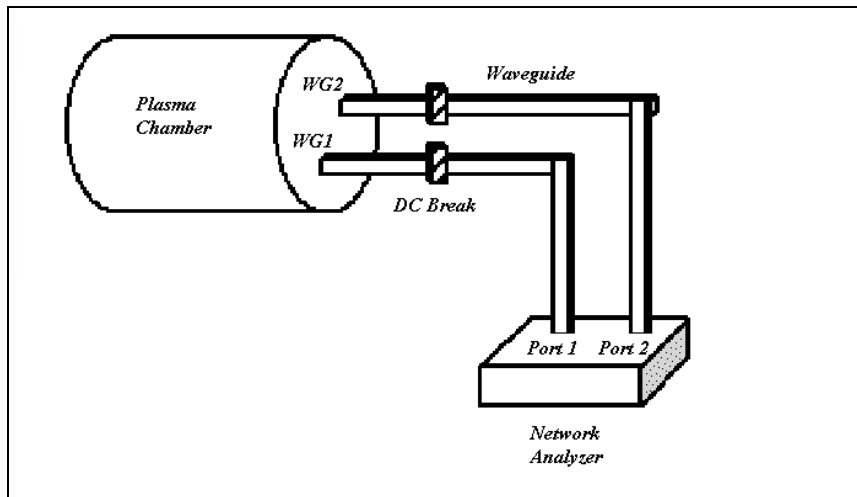


Figure 5: Experimental set-up for the  $S$ -parameters measurements.

The  $S_{11}$  parameter indicates the power reflected by the plasma chamber through the waveguide WG1 and the  $S_{22}$  the one reflected by the waveguide WG2, while the parameter  $S_{12}$  represents the power measured at port 1 coming from the port 2.

By analyzing these parameters it is possible to characterize the modes that exist inside the plasma chamber. In fact the frequencies for which we have the minimum values of the  $S_{11}$  or  $S_{22}$  and at the same time the maxima values of the  $S_{12}$  parameter occur, they represent modes excited by the microwaves from the waveguides WG1 and WG2 respectively.

Figure 6 represents a full scan in the whole operating range. Below 9 GHz the cut-off of the WR62 waveguide occurs, consequently there is no longer wave propagation inside it, consequently, we are not able to experimentally validate the results reported in table 1. For this reason we concentrated our efforts in investigations mainly around the frequency of 14 GHz

which is a source value often used during normal operations; results and comments at higher frequencies will also be presented.

Figure 7 and 8 show, respectively, the measured data in a narrow range around 14 GHz (13.95-14.05 GHz). It must be remarked that we have a point each 125 kHz

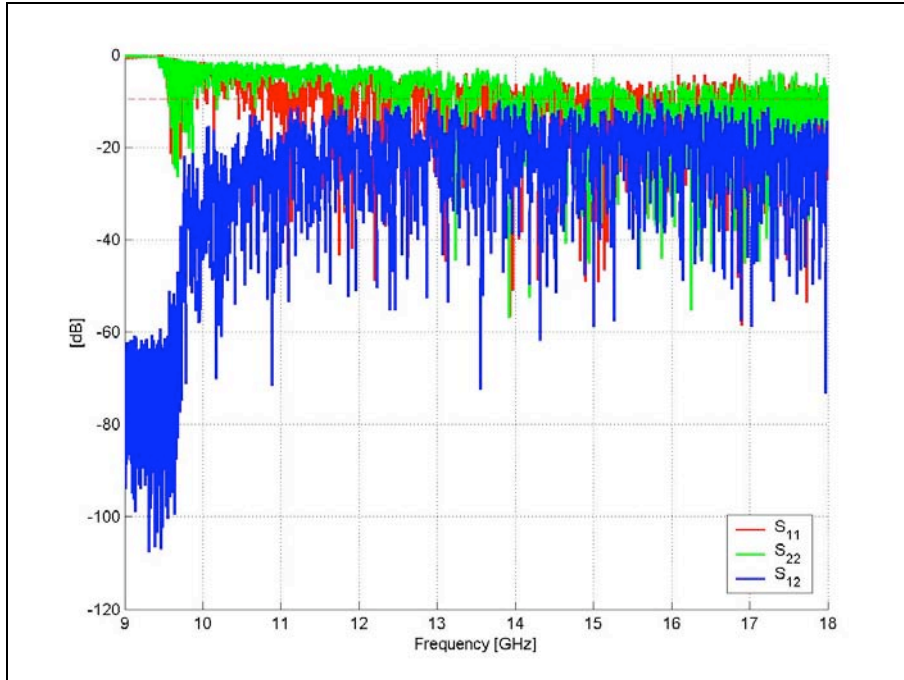


Figure 6: Measured scattering parameters in the 9-18 GHz frequency range.

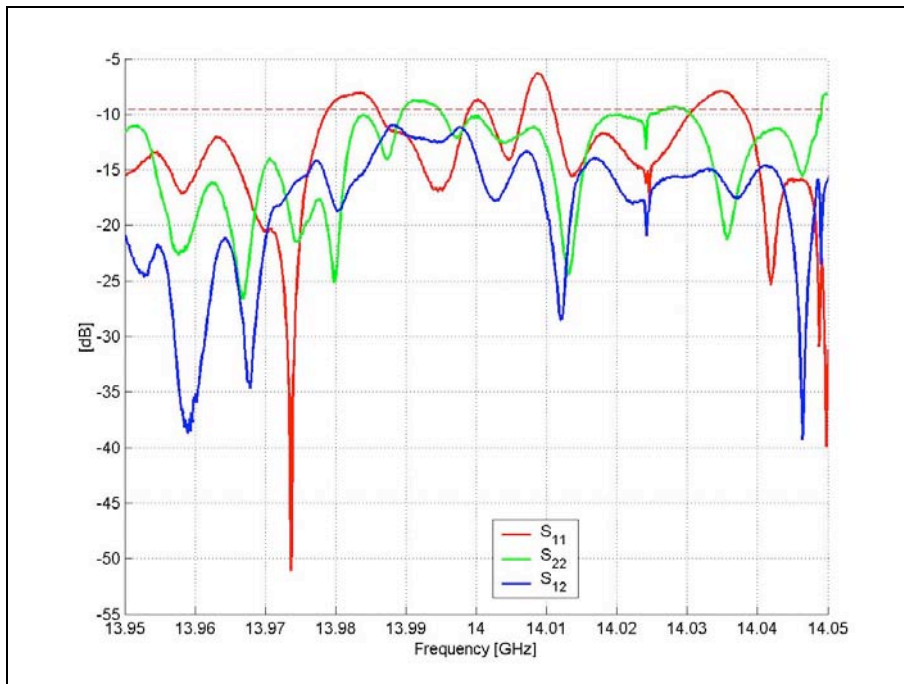
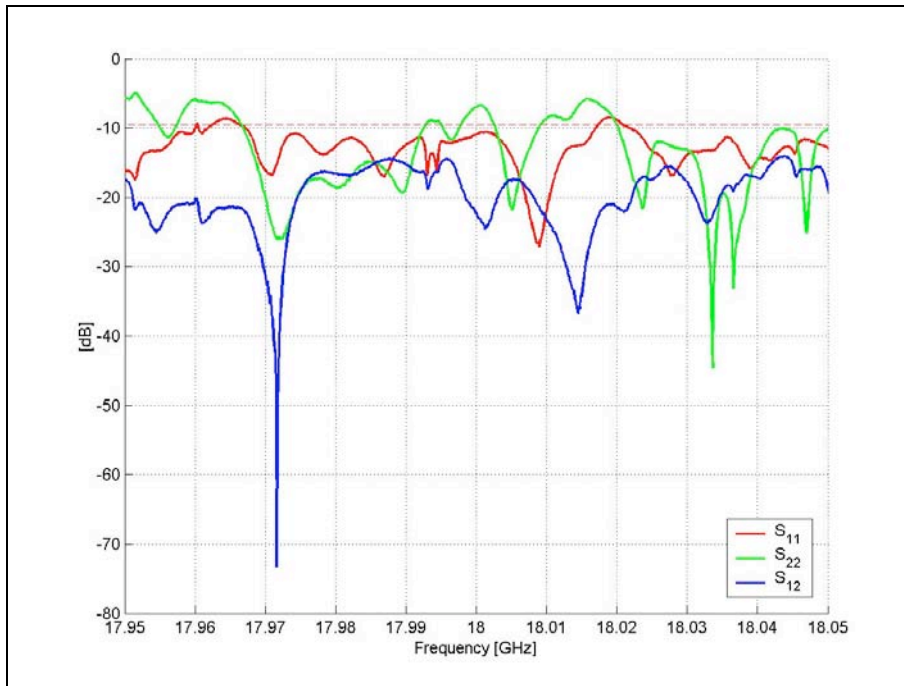


Figure 7: Measured scattering parameters at 14 GHz.



*Figure 8: Measured scattering parameters at 18 GHz.*

These parameters were measured without the DC-Break (a 0.5 mm thick TEFLON foil) which isolates the microwave generators from the source plasma chamber that it is maintained at high voltage. The effect of the DC-Break on the coupling is shown in the figures 9, 10 and 11 (for frequencies near to 14 GHz) and in the figures 12, 13 and 14 (for frequencies near to 18 GHz). It can be clearly noticed that the transmitted power at both operating frequencies (figure 11 and figure 14) shows an attenuation due to the insertion of the TEFLON foil which is more critical at 18 GHz. However, in different operational points, the transmitted power remains practically unchanged at 14 GHz, then particular care must be taken in the choice of the operating frequency to avoid losses. In general, by looking to the pictures 9-14 it seems that there is no influence on the resonating frequencies, while a clear mismatch is introduced in both ranges.

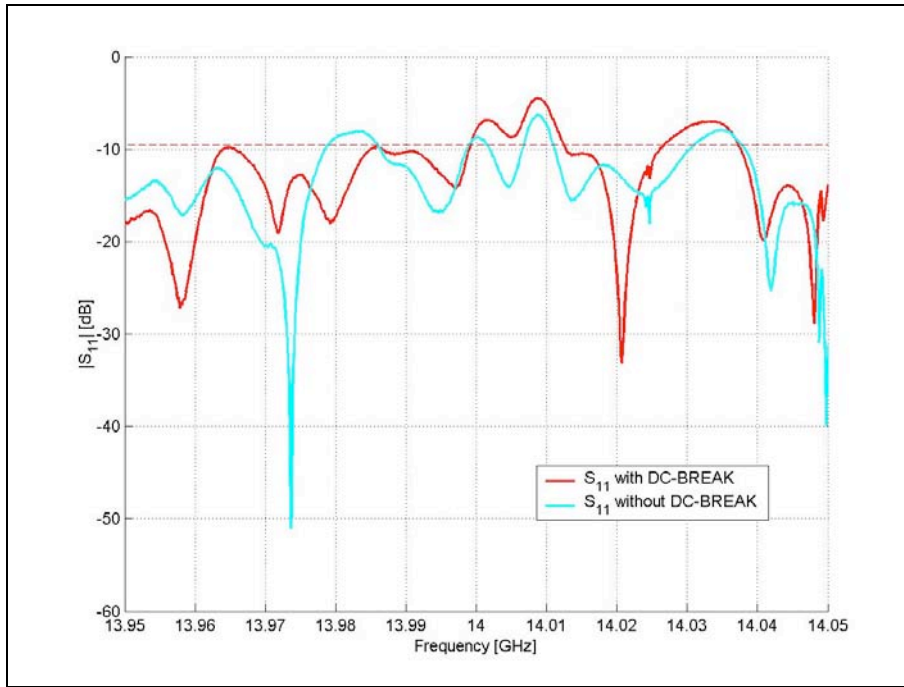


Figure 9: Effect of the DC-Break on the waveguide WG1 at 14 GHz.

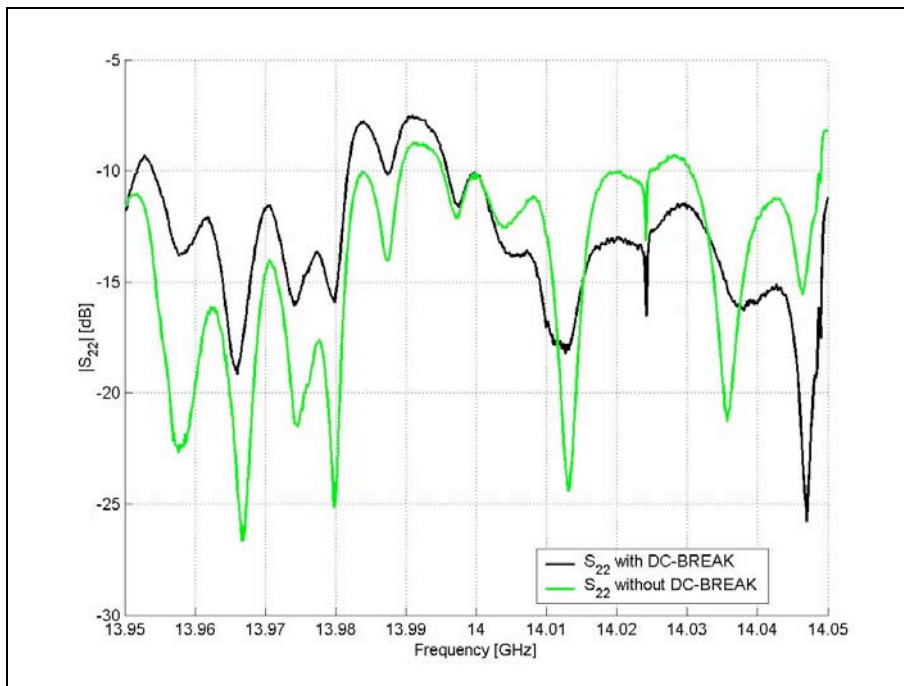


Figure 10: Effect of the DC-Break on the waveguide WG2 at 14 GHz.

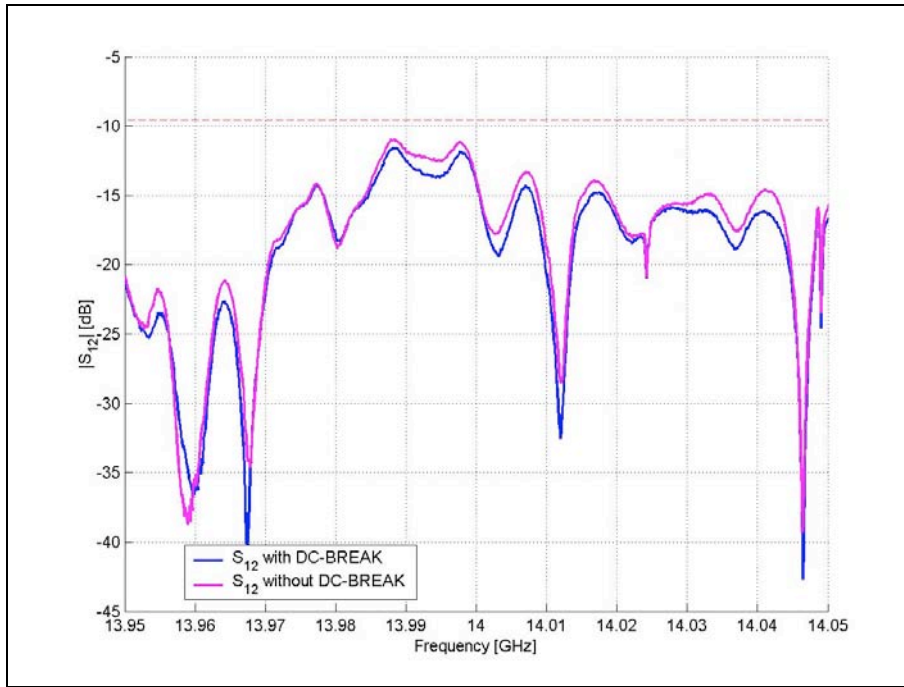


Figure 11: Effect of the DC-Break on the  $S_{12}$  at 14 GHz.

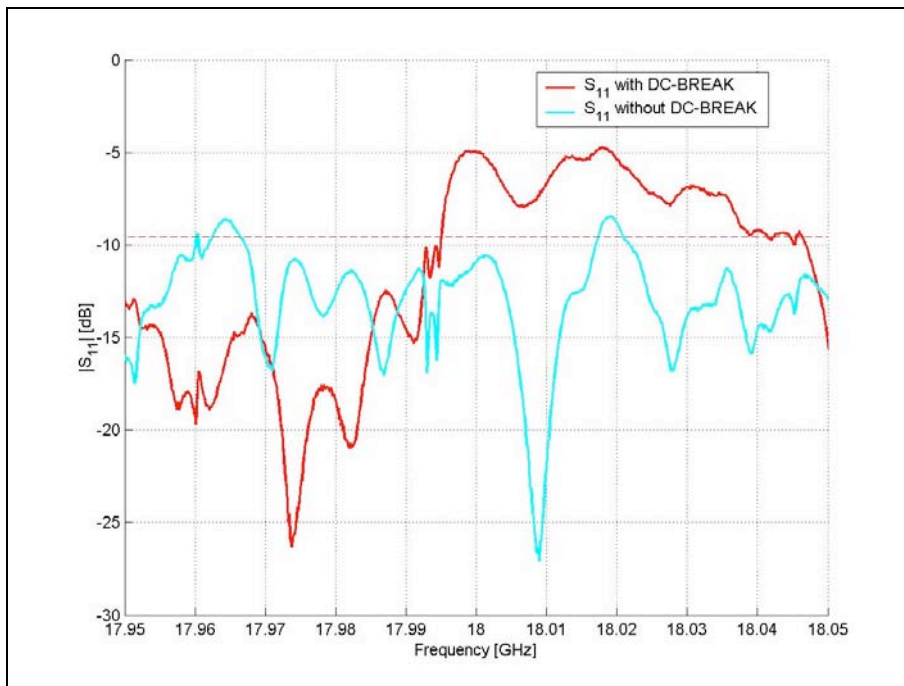


Figure 12: Effect of the DC-Break on the waveguide WG1 at 18 GHz.

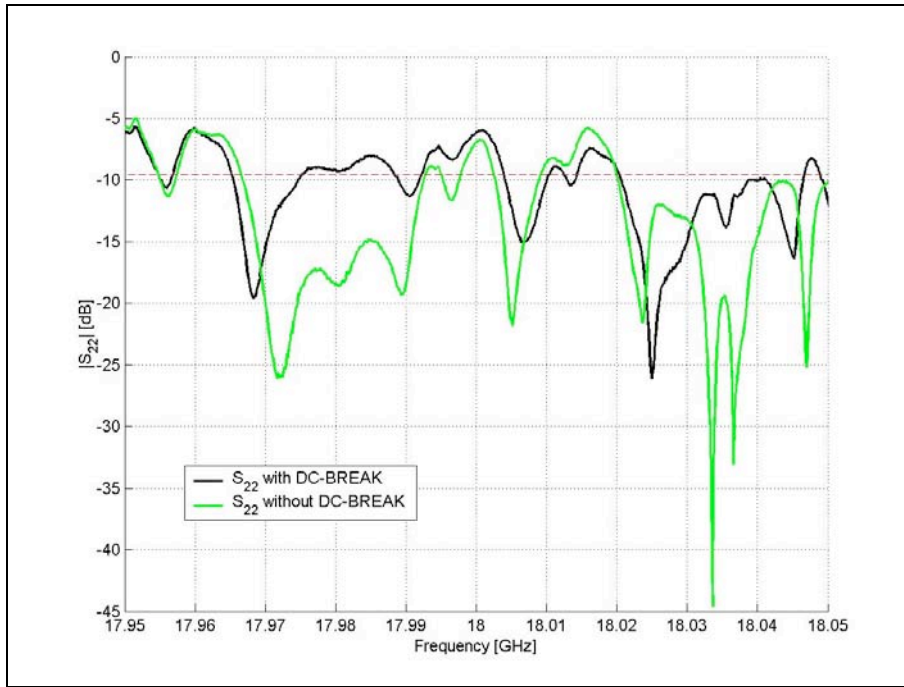


Figure 13: Effect of the DC-Break on the waveguide WG2 at 18 GHz.

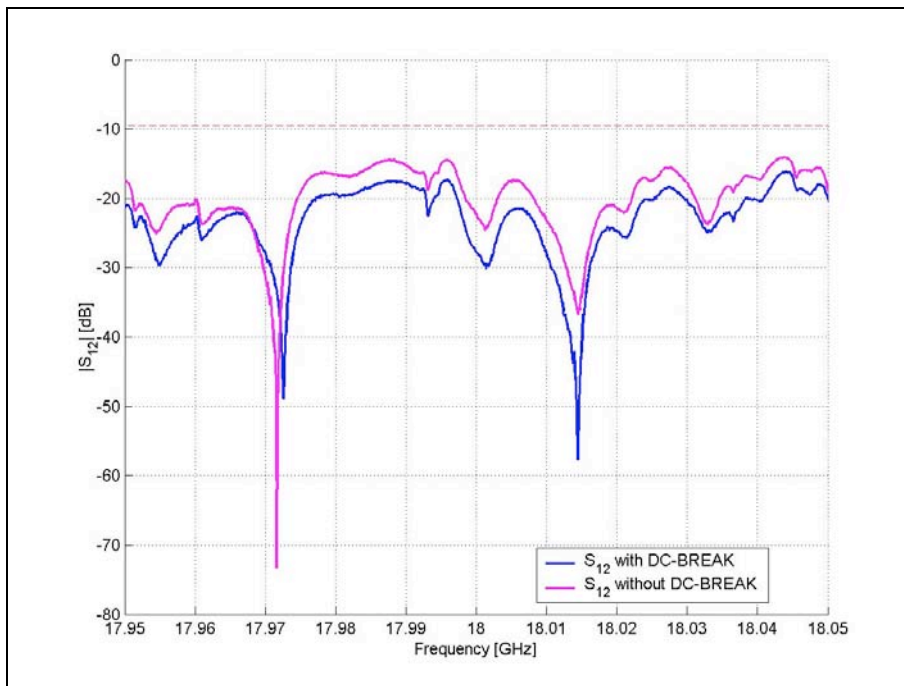


Figure 14: Effect of the DC-Break on the  $S_{12}$  at 18 GHz.

#### 4. Comparison between experimental and simulated scattering parameters

As reported in section 2, specific characteristics of CST MWS simulator in the eigenmodes domain do not allow to perform simulations with open structures, and for this reason our model of the plasma chamber (considered as a completely closed cavity) is oversimplified. However a rather simple approach to the open cavity problem consists of the use of a time domain analysis including waveguide ports [4]. These waveguides boundary ports are used to simulate an infinitely long waveguide, e.g. a rectangular waveguide, a coaxial cable or a micro strip line. These ports need to be located at the boundaries of the calculation domain and will then be automatically extended to infinity [1]. As we have performed a series of experimental measurements of the S-parameters, it is possible to compare simulated and measured data taking into account a more accurate model of the plasma chamber, considering the two waveguides connected at the source microwaves inputs WG1 and WG2 (according to figure 1). The computation domain is discretized by an algorithm named PBA (Perfect Boundary Approximation). The discretization factor is very important for the accuracy of the simulated data, but its excessive enhancement generates a considerable increase of the simulation time. Then the coupling between the resonant cavity and the two WR62 waveguides has been simulated by using the CST MICROWAVE STUDIO Transient solver. Figure 15 shows the CST MWS workspace with the simulated structure, it consists of a resonant cavity in vacuum ( $\epsilon_r = 1$ ) with radius 65 mm and length 450 mm, with aluminum walls ( $\sigma = 3.77 \cdot 10^7$  [S/m]) which is connected with two WR62 waveguides (15.799 mm x 7.899 mm).

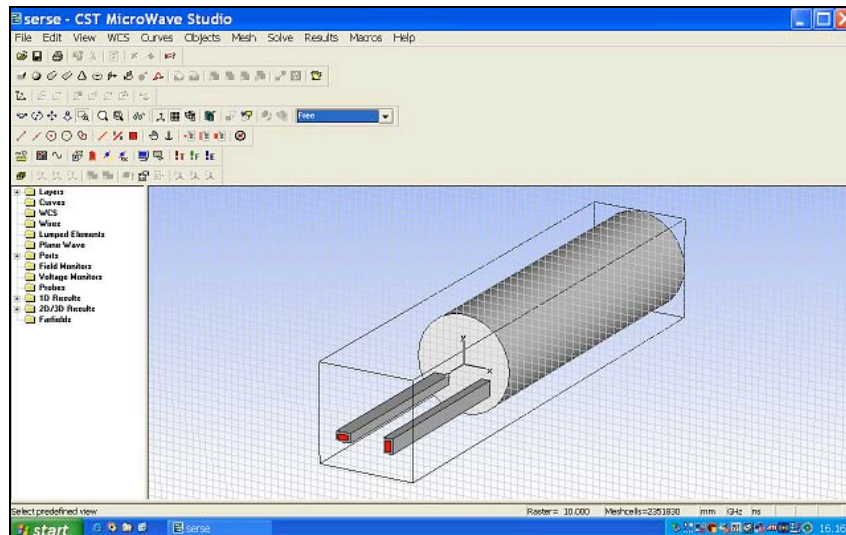


Figura 15: Main window of the CST MICROWAVE STUDIO and simulated structure.

The input signal is provided through the ports by setting the frequency range of a Gaussian pulse. The time domain solver calculates the development of fields through the time. The program calculates the answer to this pulse and, by using the Discrete Fourier

Trasform (DFT), it provides the S-parameters in the frequency domain defined as the ratio between the output signal spectrum and the input signal spectrum.[2]

In the following figures we will show the results of the simulations, remembering that the  $S_{11}$  parameter is related to the power reflected by the WG1 port, whereas  $S_{22}$  is related to the WG2 port. As before (see section 3), the frequency for which there is a minimum for  $S_{11}$  or for  $S_{22}$ , and at the same time  $S_{12}$  (or  $S_{21}$ ) has a maximum, is a resonant frequency of the cavity. Hence by combining the information about the scattering parameters it is possible to characterize completely the coupling properties of our system (plasma chamber plus waveguides).

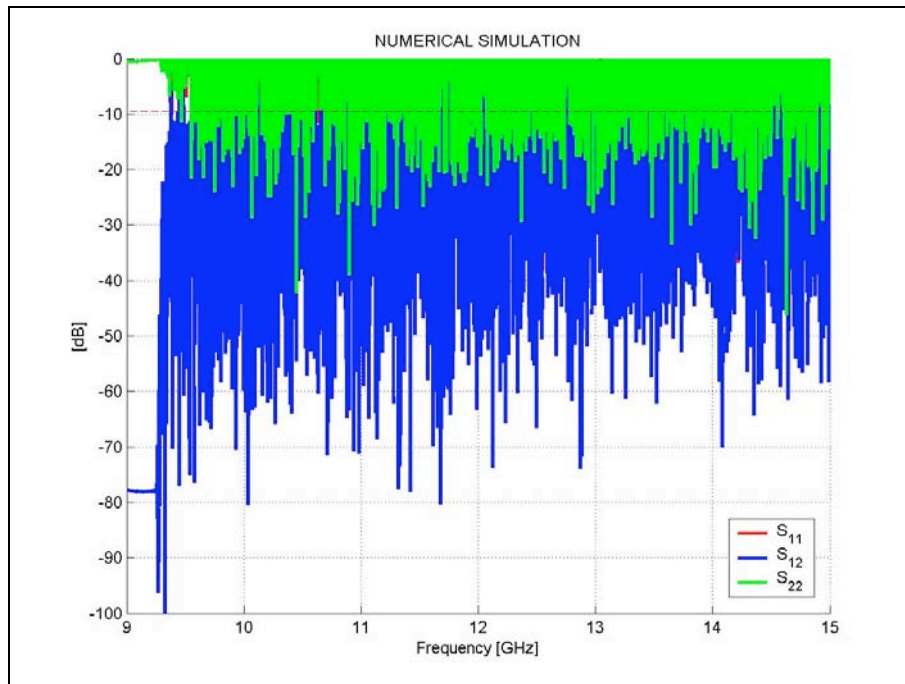


Figure 16: Simulated scattering parameters in the 9-15 GHz frequency range.

Figure 16 shows the behaviour of the four S-parameters from 9 to 15 GHz.

The  $S_{12}$  and  $S_{21}$  parameters are quite similar. It is clearly noticed that in proximity of 9.3 GHz occurs the cut-off frequency of the waveguide (for frequencies below the cut-off, wave propagation is not possible in the waveguide). Above this frequency the figure shows the presence of resonant modes. Now, it is interesting to show a comparison between simulated and measured data. We report again the figure 7 that shows the scattering parameters around 14 GHz, while the figure 18 shows a detail of the figure 16, with a frequency span of 100 MHz centred on 14 GHz.

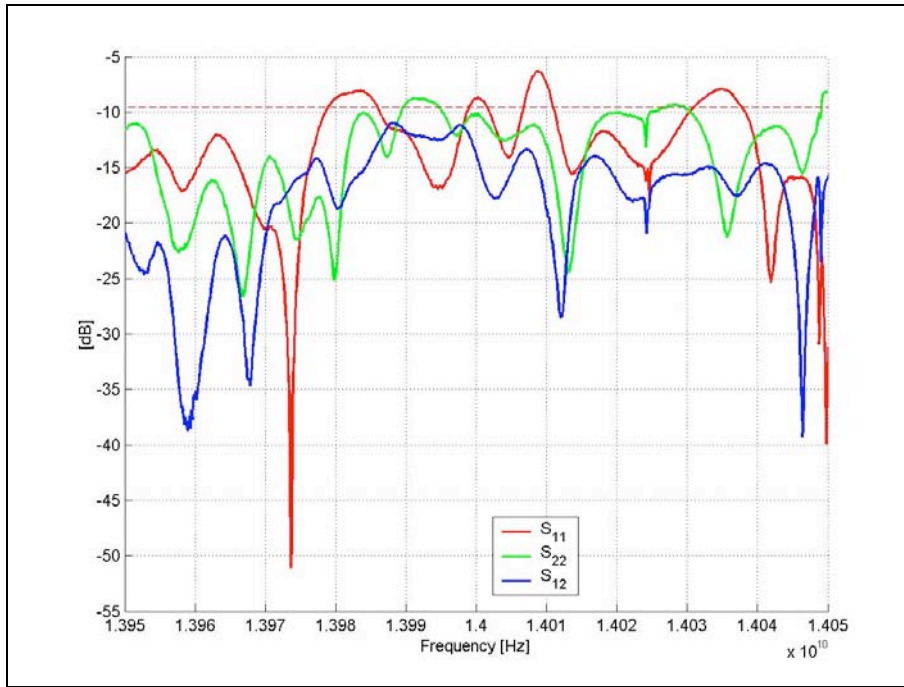


Figure 17: Measured scattering parameters at 14 GHz.

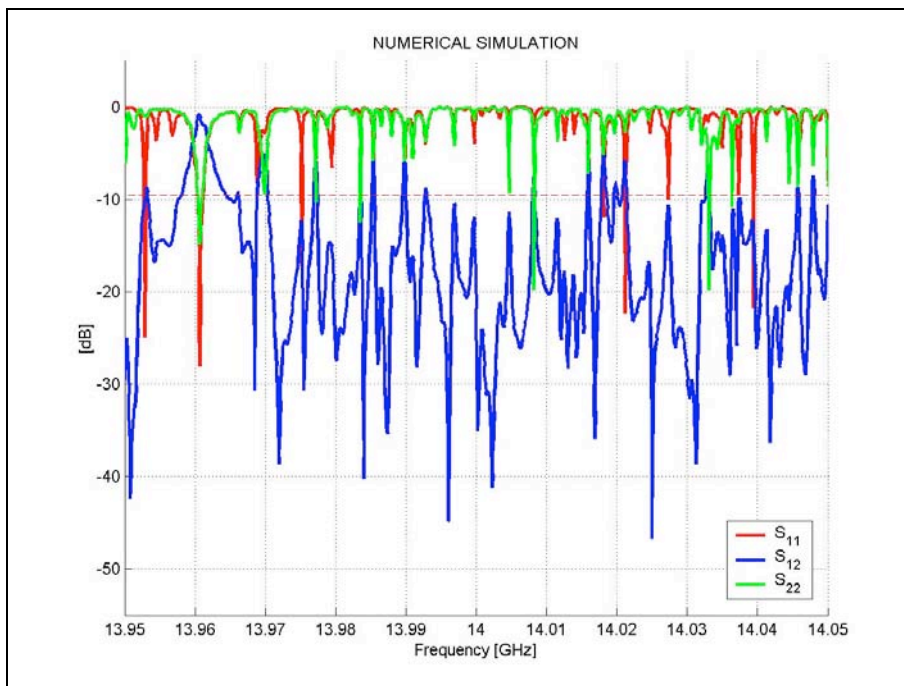


Figure 18: Simulated scattering parameters from 13.95 GHz to 14.05 GHz.

It must be pointed out that in the simulation (figure 18) we have only a point each 70 kHz while in the measure we have only a point each 125 kHz. Taking into account this

consideration it is clear that the density of modes shown in figure 17 is lower than the one shown in figure 18.

This first approach to the problem is sufficient to show that an accurate simulation of the electromagnetic properties of the plasma chamber is possible, by optimizing simulations times and plasma chamber modelling, and by using more powerful calculation tools.

## 5. Microwave generators spectrum contents

The last part of the experimental measurements is related to a spectral characterization of the microwaves that feed the plasma chamber.

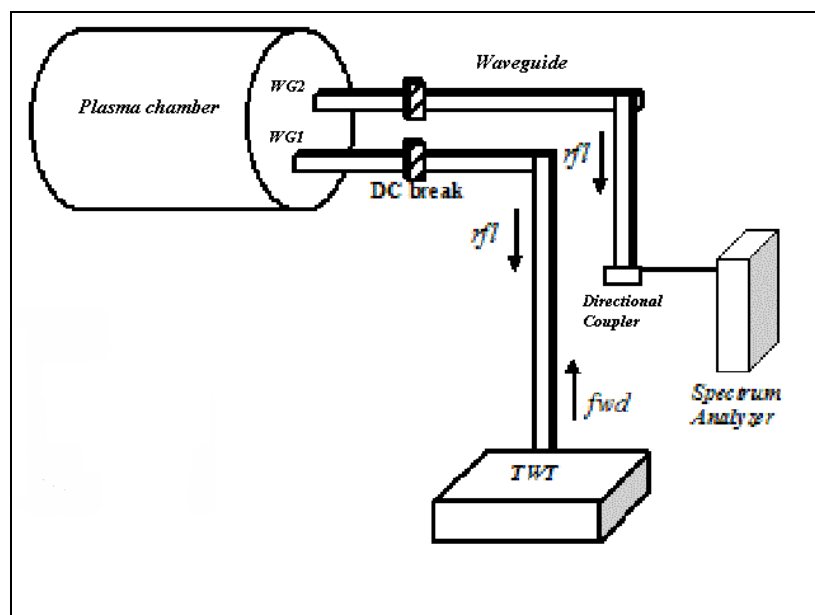


Figure 19: Scheme of the experimental apparatus.

These measurements have been performed by using the following instrumentation:

- Spectrum Analyzer HP 8565 E [4], remotely controlled through GPIB interface by Agilent VEE Pro-test 7.0 which allows to change the setting of the main measure parameters (Span<sup>1</sup> and Resolution Bandwidth<sup>2</sup>).
- HP E4444A program, employed for the analysis of the experimental spectra.
- CPI Traveling Wave Tube Amplifier (TWTA) model VZM-6993J2, with a frequency range of 8-18 GHz and 300 W maximum power.
- R&S SMP 02 Signal Generator

<sup>1</sup> Span: The frequency span defines the total amount of frequency spectrum captured by the instrument.

<sup>2</sup> Resolution Bandwidth (RBW): Controls the frequency resolution of the instrument.

At the beginning we investigated the spectra of the signal emitted by the TWTA when it is directly connected with a matched load, afterwards we connected the TWTA to the SERSE plasma chamber using the WG1 microwave port and we inspected the microwave radiation coupled to the WG2 input with the spectra (figure 19).

The spectra were obtained when a plasma was inside the source vacuum chamber. In the following the most interesting figures are shown.

Figure 20 shows a spectrum acquisition for TWTA at 14 GHz with the following parameters set-up:

SPAN = 500 Hz  
RBW = 3 Hz  
Microwave Power = 246 W  
Central Frequency = 14 GHz

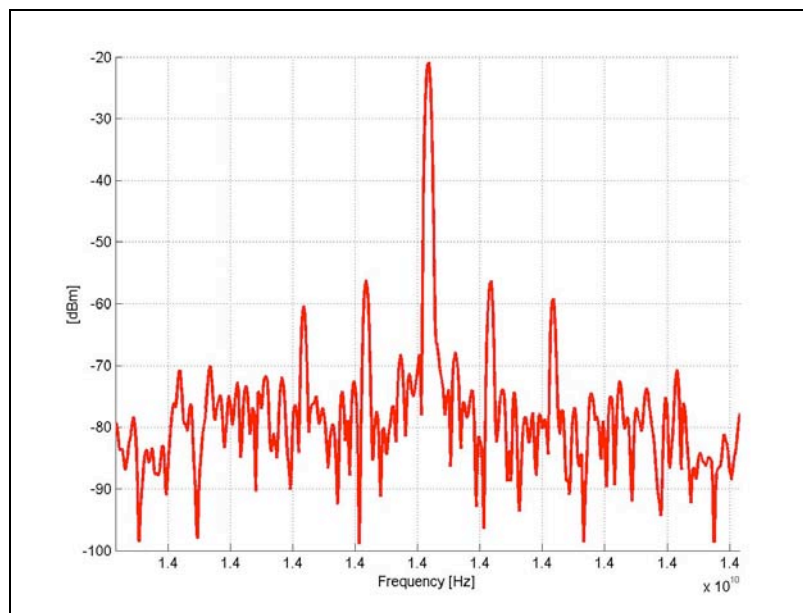


*Figure. 20: Spectrum of the microwave radiation acquired at microwave input WG2 with the TWT connected to the WG1 microwave input: Harmonic principal (14000000958,83 Hz) (14 GHz - 246 W power introduced - 16 W power reflected).*

We can notice that figure 20 features the presence of lateral peaks. The same peaks have been obtained in measurements with dummy load directly connected to the generator [6].

It is worth to notice that the lateral peaks are symmetrically displayed with respect to the main one with power ratios smaller than 35 – 45 dB, and a frequency shift of 50 Hz integer multiples.

This characteristics appears also acquiring the second harmonic of the amplified signal.

Figure 21 shows the spectrum acquired at 28 GHz, because of the low signal level we expect that this effect is weak concerning the plasma heating.

In fact the absolute level of such harmonic is about 40 dB below the principal harmonic level, so that the electric field is affected only slightly, about 1%.

SPAN = 500 Hz  
RBW = 3 Hz  
Microwave Power = 246 W  
Central Frequency = 28 GHz

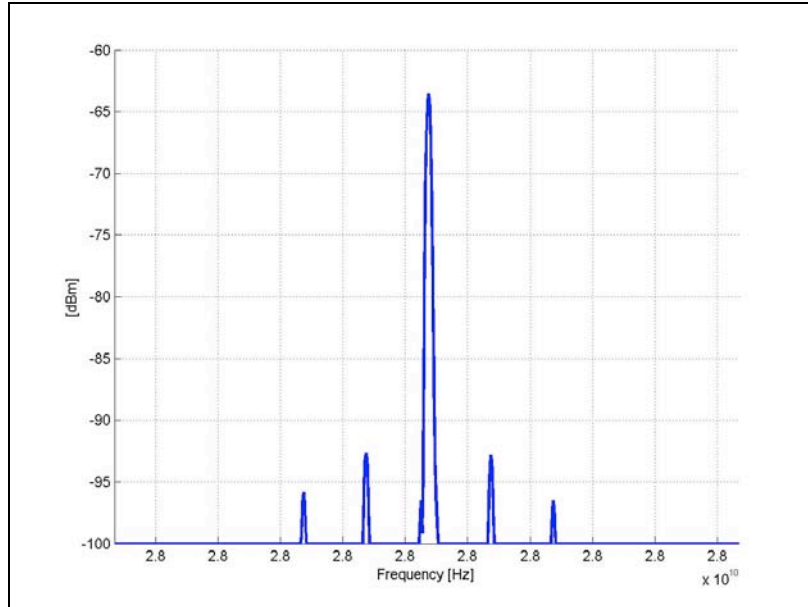


*Figure. 21: Spectrum of the microwave radiation acquired at microwave input WG2 with the TWT connected to the WG1 microwave input: Harmonic principal (28000001918,67 Hz) (14 GHz - 246 W power introduced - 16 W power reflected).*

## 6. Conclusions

The results presented in this report represent a first step towards a complete electromagnetic characterization of the plasma chamber of ECR ion sources. In particular the data shown in section 2 demonstrate that it is possible to determine numerically a limited (at present) number of cavity modes by using an oversimplified model, considering the plasma chamber without holes. The only way to simulate correctly the cavity characteristics is the time domain simulation, as seen in section 4. This technique has permitted to obtain a first rough comparison between simulated and measured data, as again observed in section 4. In order to provide more accurate results, a series of simulation will be done in the time domain by using more powerful computers, allowing a better discretization of the calculation domain. Therefore, further studies of the coupling between microwave generators and source vacuum chamber in presence of plasma are planned.

Figure 22 shows the set-up which will be employed in such measurements: a reflectometer with high isolation will be used to precisely measure the reflected power. Finally a comparison between measurements with and without plasma will make possible the study of the influence of the plasma on the electromagnetic characteristics of the SERSE ECR ion source.

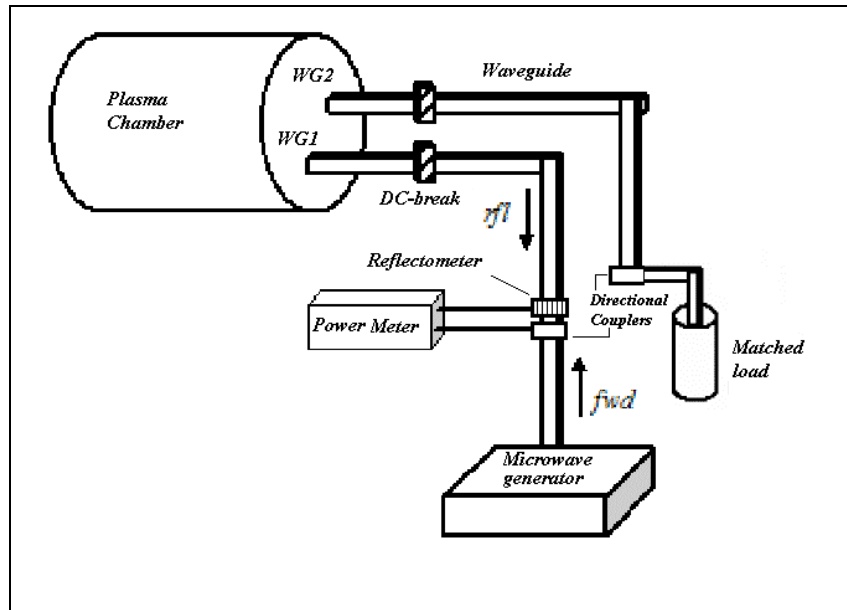


Fig. 22: Experimental set-up for the next S-parameters measurements when a plasma is present inside the ECRIS chamber.

## ACKNOWLEDGMENTS

The support of the 5<sup>th</sup> Nat. Committee of INFN through the INES experiment is warmly acknowledged.

## 7. References

- [1] CST MICROWAVE STUDIO™ User Guide.
- [2] Prof. S. Barbarino, Appunti di Microonde, 2006.
- [3] F. Consoli, S. Barbarino, L. Celona, G. Ciavola, S. Gammino and D. Mascali. Investigation about the modes in the cylindrical cavity of an ECR ion source., *Proc. Int. Conf PPLA-PIBHI, Taormina, June 2005, published in Radiating Effects and Defects in Solids, vol 160, n. 10-12 (2005), 467.*
- [4] R. Schuhmann, T. Wiland. Rigorous analysis of trapped modes in accelerating cavities. *Physical Review Special Topics – Accelerators and Beams, Vol 3, 122002, 2000.*
- [5] Spectrum Analyzer HP/Agilent 8565 E, User Guide. *HP, Agilent Technologies.*
- [6] D. Mascali, L. Celona, F. Consoli, S. Gammino, G. Ciavola and S. Barbarino. Analysis of microwave spectra emitted from TWT and Klystron-based generators used for the ECRIS at LNS, *LNS internal report.19* Gennaio 2006.